Poly(lactic acid)/Menadione Based Composite for Active Food Packaging Application

Usman Lawal[1,2,3] · Vijay Robert[1] · Sravanthi Loganathan[1,2] · Ravi Babu Valapa[1,2]

Abstract

In the current work, poly(lactic acid) (PLA) based composite films are developed via incorporation of "menadione" (MD) as additive agent and solution casting approach is followed for fabrication of composite films. The impact of MD on the physico-chemical properties of PLA and its active food packaging characteristics is envisaged herein. The incorporation of MD in the PLA matrix helps in favour of four-fold enhancement in elongation property for the composite films. Interestingly, the PLA/MD composite films demonstrate complete UV-barrier property and presents an UV protection factor (UPF) value > 50. The oxygen permeability analysis reveals that the MD could help in reducing the oxygen transmission rate by ~ 30% for PLA composites than PLA. The PLA/MD composite films act as potential 2,2-diphenyl-1-picrylhydrazyl (DPPH) scavenger by presenting ~ 97% antioxidant activity. The increase in wt% loadings of MD in the PLA matrix show improved antibacterial properties against Gram positive *Staphylococcus aureus* (*S. aureus*) and Gram negative *Escherichia coli* (*E. coli*). The PLA/MD composite films registered values within the EU limit of 10 mg/dm^2 for dry food migration. Thus, the PLA/MD composite formulation envisaged in this work presents promising characteristics pre-requisite for both watery and dry active food packaging application.

✉ Ravi Babu Valapa
  vravibabu@cecri.res.in; vravibabucecri@gmail.com

1 Electrochemical Process Engineering, CSIR-Central Electrochemical Research Institute (CECRI), Karaikudi, Tamil Nadu 630003, India

2 Academy of Scientific and Innovative Research (AcSIR), Ghaziabad, Uttar Pradesh 201002, India

3 Department of Chemical Sciences, Federal University Wukari, Taraba, Nigeria

Graphical Abstract
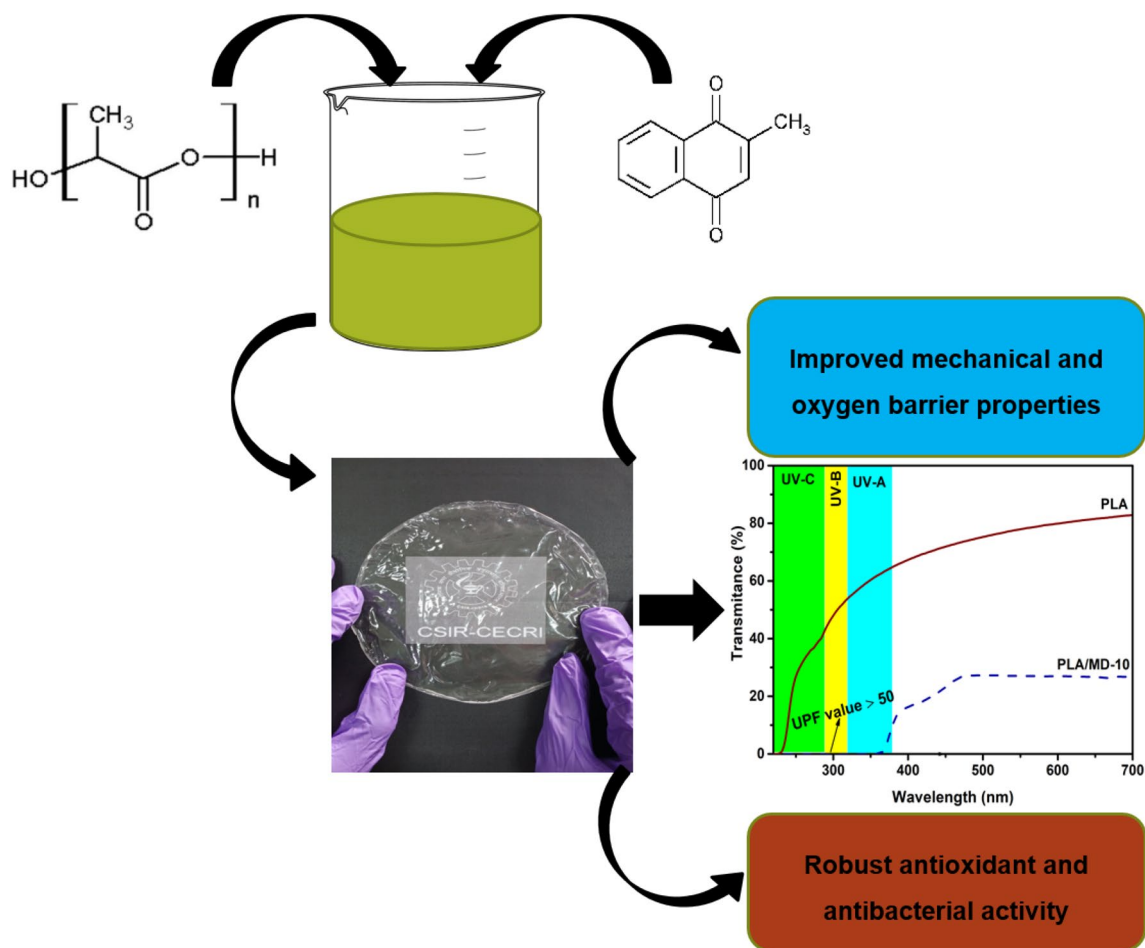
Keywords PLA · Menadione · Composite · UV-barrier · Antioxidant activity · Packaging

Introduction

In the current scenario, the plastics derived from petro-chemical resources occupy principal market in the food packaging industries. The versatility of these conventional plastics is mainly due to its easy processability, mechanical strength, and availability at affordable cost [1, 2]. However, the plastics from petrochemical origin are not environmentally benign owing to their non-biodegradable nature [3]. Recently, poly (lactic acid) (PLA) has emerged as the potential biopolymer in the packaging industry due to its good tensile strength, biocompatibility, and biodegradability under composting conditions [4, 5]. However, PLA exhibits certain drawbacks like brittleness, slower rate of crystallization, deprived gas barrier as well as UV protective characteristics, and poor anti-bacterial property which limits its usage in commercial application in terms of food packaging [6, 7].

In order to overcome the limitations associated with PLA, strategies like blending of PLA with other polymers or incorporation of different additives in the PLA matrix are followed. The blending of PLA with other polymers like PLA/cellulose and PLA/Polybutadiene-ABS has been shown to enhance the mechanical as well as physical characteristics of PLA [8, 9]. In the case of PLA composites, incorporation of ZnO, β-cyclodextrin and *Phoebe zhennan* extracts has been found to provide improvement in the mechanical, physical and barrier properties [10, 11]. Shang et al. reported that the addition of wood fibre in PLA resulted in ~100% UV blockage with good transparency [12]. Similarly, Ke et al. [13] reported that functionalising PLA with bamboo fiber resulted in high heat resistance and almost complete UV rays blocking. Further, Xu et al. demonstrated how quantum dots derived from coffee ground induced antibacterial effect in PLA matrix [14]. However, the enhancement in terms of food packaging properties is mainly dependent on

homogenized state of filler reinforced in the biopolymer matrix. In the current scenario, exploration of new types of additives in the PLA matrix has received considerable attention in order to improve the active food packaging properties [15, 16]. Apart from improving the physico-chemical properties, it is necessary to improve the functional properties like antibacterial, antioxidant, and UV barrier characteristics. The active food packaging properties will aid in the extension of shelf-life for stored food product via prevention of food from spoilage [17, 18].

The current work aims to use menadione (MD) as functional additive in the PLA matrix and explore its active food packaging characteristics, which has not been documented earlier in the best of our knowledge. Menadione or Vitamin K_3 is the synthetic compound that falls under the category of lipid-soluble vitamins, which converts its form into Vitamin K_2 in the gut [19]. Menadione is known to demonstrate antibacterial action against multi-drug resistant bacteria like *Staphylococcus aureus* (S. aureus) and *Escherichia coli* (*E. coli*) [20]. In addition to this, menadione is reported to exhibit strong antioxidant activity [21]. The other derivatives of vitamin K are known to exhibit UV absorption properties [22]. All these characteristics suggest that menadione can be explored as functional additive in the PLA matrix. The influence of wt% loadings of MD on the physico-chemical characteristics like thermal stability, crystallization behaviour, and ductility are investigated in the present work. The PLA/MD composites are further emphasized for its active food packaging characteristics like oxygen barrier, UV absorption, anti-oxidant, and anti-bacterial efficiency. The PLA/MD composites fabricated in the current work demonstrates complete UV blockage and effective anti-bacterial property against the most pathogenic food borne bacterial like *E. coli and S. Aureus*. In addition to this, the incorporation of MD in the PLA matrix plays excellent role in terms of antioxidant activity. All these features speculate that the PLA/MD composite may be a viable option for active food packaging application.

Materials and Methods

Materials

Poly (lactic acid) (Grade: PLA 4043D) was acquired from NatureWorks LLC, Ingeo™ Biopolymer 4043D, USA and utilized as bio-polymer matrix. Menadione or Vitamin K_3 (IUPAC name: 2-methyl-1,4-naphthoquinone, Appearance: solid crystalline, Empirical formula: $C_{11}H_8O_2$, MW: 172.18 g/mol, and MP: 105 °C) was used as additive in the PLA matrix. In this work, 2, 2-diphenyl-1-picrylhydrazyl (DPPH) was utilized as antioxidant analyzer. Both of them were supplied by Sigma-Aldrich, USA. The chloroform was

supplied by Sisco Research Laboratories, India and used as solvent during the fabrication of PLA and PLA/MD composite films. The Tenax was procured from Sigma-Aldrich, USA and utilized as dry food simulant during migration analysis.

Preparation of PLA/Menadione Composite Films

The PLA/MD composite films were fabricated via the solvent casting method. Initially, different amounts of menadione (MD) (1, 3, 5, and 10 wt% based on pure PLA) were added into 30 mL of pure chloroform and subjected to homogenization at 50 ºC using a magnetic stirrer for an hour until complete dissolution of MD in the chloroform solution. Around ~ 1 g of PLA was dissolved in 70 mL of chloroform for 1.5 h using a magnetic stirrer at room temperature. Followed by this, the MD/chloroform solution was then transferred into PLA/chloroform solution prepared in the previous step. The resultant PLA/MD/chloroform solution was then allowed to homogenization for 1 h at 50 ºC. The homogenized solution thus obtained was then casted onto flat petri dish and allowed for evaporation of the solvent under ambient condition for 24 h. The thin PLA/MD composite film was carefully peeled off from the petri dish and vacuum dried at 40 °C for 48 h to remove any traces of chloroform. The final films were free standing and of uniform thickness (50 ± 5 μm). The films were designated as PLA/MD-1, PLA/MD-3, PLA/MD-5, and PLA/MD-10 in accordance with the wt% loadings of MD in the PLA matrix. In the case of fabrication of PLA film, PLA/chloroform solution obtained after dissolution of PLA in the chloroform was casted onto flat petri dish. Apart from this, rest of the procedure remains unaltered for fabricating PLA film.

Characterization

Thermogravimetric Analysis (TGA)

The thermal decomposition profile for PLA and PLA/MD composites was obtained using thermal analysis carried out using TG analyser (NETZCH, Germany & Model: STA 2500). For this purpose, 5 ± 0.2 mg of PLA and PLA/MD composite samples were weighed and subjected to thermal analysis in the temperature regime of 25 to 600 °C at a heating rate of 10 °C/min. The thermal analysis was allowed to occur under Nitrogen (N_2) atmosphere at a flow rate of 100 mL/min.

Differential Scanning Calorimetry (DSC) Analysis

The thermal properties [glass transition temperature (T_g), cold crystallization temperature (T_{cc}), melting temperature (T_m)] for PLA and PLA/MD composite samples were analysed using DSC analyser (METTLER TOLEDO,

Switzerland & Model: DSC 1). For this analysis, 5 ± 0.2 mg of PLA and PLA/MD composite samples were weighed and hermetically sealed in aluminium pans. The samples were heated from 25 to 180 °C at a heating rate of 5 °C/min under N_2 atmosphere and held isothermally at 180 °C for 5 min in order to erase their thermal history during the first heating cycle. The thermal analysis was allowed to take place under N_2 atmosphere at a flow rate of 100 mL/min. The thermal properties for PLA and PLA/MD composite samples were derived from the second heating cycle. The degree of crystallinity $[X_c]$ for PLA and PLA/MD composite samples was calculated using the following Eq. (1) [23].

$$X_c(\%) = \left[\frac{\Delta H_m - \Delta H_c}{\Delta H_0^m} \right] \times \frac{100}{m} \qquad (1)$$

where ΔH_c is the enthalpy of crystallisation, ΔH_m is the enthalpy of fusion and, 'm' represents the weight fraction of PLA in the sample, ΔH_0^m represents 100%theoretical enthalpy of PLA, which corresponds to 93.6 J/g [24].

X-Ray Diffraction (XRD) Analysis

The diffraction pattern for PLA and PLA/MD composite samples were obtained using XRD analyser (Bruker, Germany & Model: D8 Advance). The XRD data for PLA and PLA/MD composite samples was obtained in the 2θ ranging from 5 to 50° with a scanning rate of $3° \, s^{-1}$. The diffraction analysis was performed under ambient environment and the equipment was operated at 40 kV and 30 mA.

Fourier Transform Infrared (FTIR) spectroscopy

The IR spectra for PLA and PLA/MD composite samples were obtained using FTIR spectroscopy (Bruker, Germany & Model: TENSOR 27) and the equipment was operated under attenuated total reflectance (ATR) mode. The IR measurements for PLA and PLA-MD composite samples were made in the wavenumber regime of 4000–400 cm^{-1} with a resolution of 4 cm^{-1}.

Morphological Analysis

The morphological analysis for MD was carried out using field emission scanning electron (FESEM) microscopy (Carl Zeiss, Germany & Model: 27 PerkinElmer Spectrum Two). Further, the nature of dispersion of MD in the PLA matrix was examined via FE-SEM analysis. Prior to imaging, the samples were gold sputtered for 120 s under vacuum condition.

UV–Visible Spectrophotometry Analysis

The transparency measurement for PLA and PLA/MD composites was carried out using UV–Visible spectrophotometer (SHIMADZU, Japan & Model: UV-3600 plus). The analysis was carried out in the wavelength regime of 200–800 nm for PLA and PLA/MD composites.

Mechanical Analysis

The mechanical properties of PLA and PLA/MD composite films including tensile strength (TS) and elongation-at-break (EB %) were measured using a universal testing machine (Tinius Olsen, USA & Model: H5K). The samples for testing were prepared in accordance with the ASTM D882 standard method. The grip separation was set at 20 mm and crosshead speed of 20 mm/min was maintained until failure. The elastic modulus (EM) was determined from the slope of the stress–strain curve for each film. Three specimens of each sample were tested and the mean values were reported.

Oxygen Transmission Rate (OTR) Analysis

The oxygen (O_2) permeation analysis for PLA and PLA/MD composite was carried out with the aid of a gas permeability tester (M/S Labthink, China & model: PERME VAC-VBS). During the analysis, the temperature condition and relative humidity were maintained to be ~ 30 °C and $\sim 50\%$, respectively. The inlet pressure for O_2 was set to be 5 bar and the test regime was between 0.1 and 100,000 cm^3/m^3. 24 h. 0.1 MPa. For OTR analysis, the samples were prepared according to ASTM D1434 standard and proportional mode was followed during the test. Triplicate samples were used at a time for each analysis and an average OTR value was acquired.

Antioxidant Activity

The free radical scavenging activity (RSA) for PLA and PLA/MD composite films was evaluated using 2,2-diphenyl-1-picrylhydrazyl radical (DPPH) method [25, 26]. For this analysis, ~ 100 mg of each sample was immersed into 10 mL of DPPH/methanol solution and allowed for 24 h of incubation at room temperature. Pure DPPH solution was used as control during the analysis. After the completion of incubation period, absorbance was measured (at 517 nm) using UV–Visible spectrophotometer (SHIMADZU, Japan & Model: UV-3600 plus). The antioxidant activity of PLA composites were calculated using the following formula.

$$RSA(\%) = \left[\frac{(Ac - As)}{Ac} \right] \times 100 \qquad (2)$$

where A_c and A_s are the absorbance of DPPH control and sample, respectively. The antioxidant activity measurement was performed in triplicate runs for each sample.

Antibacterial Studies

The antibacterial activity for PLA and PLA/MD composites was studied against Gram negative *E. coli* CICC10670 and Gram positive *S. aureus* (food-borne pathogenic bacteria) using viable colony counting method following the procedure described in [26]. Initially, the bacterial stock solution was prepared by culturing the respective bacterial colonies in Luria Broth (LB) medium [1.0 g tryptone, 0.5 g yeast extract powder, 1 g NaCl dissolved in 100 mL of deionized water] at 37 ºC. Colony counting method was used to determine the initial concentration of *E. coli* and *S. aureus*, which corresponds to 3.7×10^7 and 4.5×10^7 CFU/mL, respectively. After serial dilution, 100 μL of bacterial inoculum was added to 50 mL of LB medium containing 200 mg of PLA and PLA/MD composites and incubated subsequently for 18 h. After proper dilution, the bacterial samples were plated in LB agar and viable cell count was determined. The antibacterial test was performed in triplicate runs for each sample.

Migration Analysis

The migration analysis for PLA and PLA/MD composite films was carried out using Tenax as dry food stimulant via following the established procedure [27, 28]. The guidelines for migration analysis were followed in compliance with EU FCM Regulation (EU) 10/ 2011. For the analysis, ~ 20.0 mm of test samples were covered with 80 mg of Tenax, with 40 mg on each side and placed in a clean petri dish. The samples were then subjected to heating at 70 °C for 2 h. Once the heating process was completed, the samples were allowed for cooling until the temperature was found to attain ambient range. Followed by this, each sample was weighed and the overall migration of MD into Tenax was derived by

$$M = \left[\frac{(m_o - m_f)}{S} \right] \times 1000 \tag{3}$$

where M is the overall migration (mg/dm^2), m_o is the initial mass of Tenax before the migration test (mg), m_f is the final mass of Tenax after the migration test (mg) and S is the surface area of composite films (dm^2). An average of three measurements was reported for each sample.

Menadione Release Test

The menadione release test for PLA/MD composite films was performed according to the procedure described

by Roy and Rhim [26]. For this analysis, the test sample (2.5 cm × 2.5 cm) was transferred into conical flask containing 20 mL of distilled water and allowed for incubation at 37 °C for 24 h. At regular intervals (0, 24, 48, 72 and 96 h), ~ 2 mL of the solution was collected for recording absorbance at 420 nm with the aid of UV–Visible spectrophotometer (SHIMADZU, Japan & Model: UV-3600 plus). The quantity of MD released was obtained from standard curve and expressed in μg MD/mm^2 of the film. An average of three measurements was reported for each sample.

Hydrolytic Degradation

The hydrolytic degradation of PLA and PLA/MD composite films was carried out under different temperature conditions (35 ± 1 °C and 55 ± 1 °C) in three different pH solutions, acidic pH (~ 2 ± 0.2), neutral pH (~ 7 ± 0.2) and basic pH (~ 12 ± 0.1). HCL and NaOH were used to correct the pH of the solutions. The samples were initially weighed before immersing into the solutions for 24 h. Followed by this, the samples were taken out and subjected to washing with distilled water, dried at 40 °C for 6 h and weighed again. The changes in weight before and after the degradation was calculated to determine residual weight (Ø). The residual weight (Ø) for each sample was calculated using Eq. (4).

$$\phi = \frac{w_t}{w_0} \times 100\% \tag{4}$$

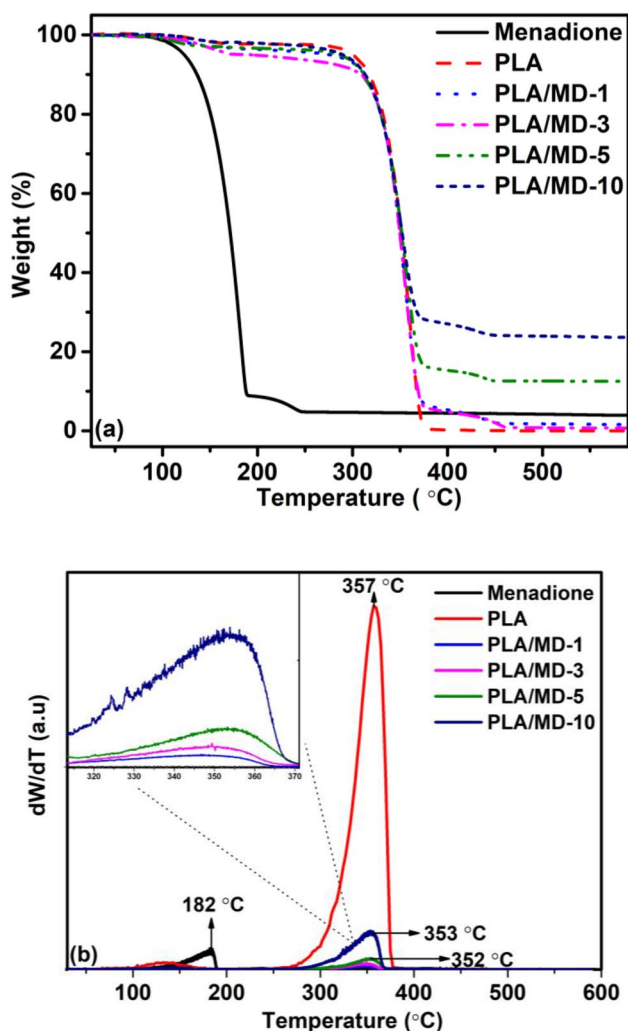where W_0 and W_t represents the weight before and after degradation of the samples at 24 h time interval.

Statistical Analysis

All the analysis was replicated thrice and their results were reported as mean ± standard deviation (S.D.). For statistical analysis, GraphPad prism® version 7.0 software was utilized. Statistical significance of the data was deduced using one way ANOVA test. Values with $*p < 0.05$, $**p < 0.01$, $***p < 0.001$ and $****p < 0.0001$ were considered as significant (where, $n = 3$).

Results and Discussion

TG Analysis

The TG curve obtained for MD, PLA and PLA/MD composites is shown in Fig. 1. It can be seen from Fig. 1 that the main degradation for MD occurs below 200 ºC, which corresponds to ~ 90% weight loss in this region. Followed by this, a small region of weight loss (~ 5%) can be noticed in the temperature regime of 190 ºC to 290 ºC. Beyond this

Fig. 1 **a** TG and **b** DTG curves for MD, PLA and PLA/MD composite films

Table 1 TGA results for MD, PLA and PLA/MD composites

Samples	$T_{10\%}$ (°C)	$T_{50\%}$ (°C)	T_{max} (°C)	Residue (%)
Menadione	136	171	182	4.8
PLA	317	351	357	0.3
PLA-MD-1	310	348	350	1.1
PLA-MD-3	311	349	351	0.9
PLA-MD-5	312	351	352	13
PLA-MD-10	313	352	353	24

50% weight loss occurs) from the TG curve as well as T_{max} (temperature at which maximum degradation occurs) from the DTG curve obtained for respective films. The T_{onset}, $T_{50\%}$, T_{max} and residue (%) obtained for MD, PLA and PLA/MD composites are reported in Table 1. It can be seen from Table 1 that the PLA exhibits T_{onset} at 317 °C. In the case of PLA/MD composites, the T_{onset} is found to decrease with respect to wt% loadings of MD in the PLA matrix. However, the $T_{50\%}$ and T_{max} values obtained for PLA/MD composites do not show much deviation as compared to PLA. Interestingly, it can be observed from Table 1 that the residue (%) is found to increase for PLA/MD composites with rise in the wt% loadings of MD in the PLA matrix. This may be due to the formation of thermally resistive char on the surface of PLA/MD composites. This in turn leads to the protection of bulk material during thermal degradation process. Similar results have been reported by Liu et al. in which the increase in wt% of filler concentration led to increase in the wt% of thermally resistive char formation [31].

DSC Analysis

The DSC thermographs obtained for PLA and PLA/MD composites during the second heating cycle are presented in Fig. 2. It can be noticed from Fig. 2 that the glass transition temperature (T_g) for PLA occurs at 62 °C. When 10 wt% of MD is incorporated in the PLA matrix, significant reduction in the T_g value is observed in comparison with PLA. The reduction of ~ 5 °C in the T_g is noticed for PLA/MD-10 composite, which may be due to the plasticizing effect provided by the filler. From the DSC thermograph, it can be seen that the exothermic region corresponds to cold crystallization temperature (T_{cc}) for PLA and PLA/MD composites. In the case of PLA and PLA/MD composites, T_{cc} can be visualized at 97.5 °C except for 10 wt% loading of MD in the PLA matrix. The prominence of the cold crystallisation peaks in the PLA/MD composites is evidence of increased crystallisation with the exception of PLA/MD-10 [32]. Moreover, the PLA/MD-10 composite exhibits higher T_{cc} at 126.6 °C compared to neat PLA and PLA/MD composites, which indicates slower diffusion rate of PLA chains to the surface of the nucleus during the
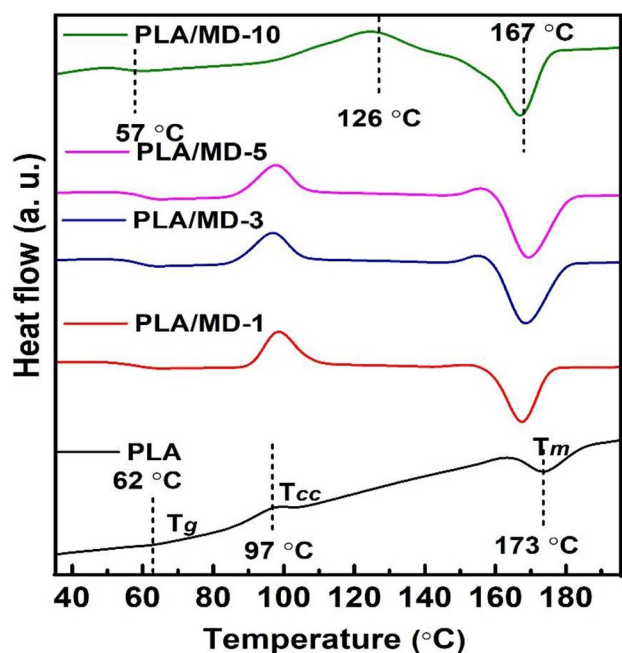
point, ~ 4.8% of total mass of MD is noticed to be remaining, which confirms the formation of char residue during the degradation of MD. It can be seen from Fig. 1 that the TG curve with regard to the PLA shows two stages of degradation. The initial weight loss observed in the temperature regime of 100–150 °C corresponds to the removal of moisture present in the sample. The second region of weight loss for PLA is recorded between 300 and 380 °C, which is attributed to the thermal degradation due to trans-esterification reaction that cleaves the PLA backbone structure [29, 30] obtained for respective films. The thermal degradation profile for PLA/MD composites also exhibits similar stages of degradation like PLA. Additionally, the changes in the thermal stability that occurs during the degradation of PLA and PLA/MD composite samples could be well understood by interpreting the T_{onset} (temperature of decomposition when 10% weight loss occurs) and $T_{50\%}$ (temperature of decomposition when

Fig. 2 DSC thermographs for PLA and PLA/MD composites obtained during second heating cycle

crystallization process [33]. The increment in the T_{cc} value along with widening of its peak width is noticed for PLA/MD-10 composite in comparison with PLA and other PLA/MD composites. This phenomenon reveals slower rate of crystallization process in the case of PLA/MD-10. The increment in T_{cc} noticed for PLA/MD-10 composite might also be attributed to the formation of ordered PLA crystals in α-form [33]. It can be observed from Fig. 2 that the PLA exhibits a melting point of 173 °C while the PLA/MD composites present unimodal endothermic peak in the melting region of 167 °C. The thermal properties of PLA and PLA/MD composites derived from DSC thermographs including glass transition temperature (T_g), cold crystallisation temperature (T_{cc}), melting temperature (T_m), enthalpy of fusion (ΔH_m) enthalpy of cold crystallisation (ΔH_{cc}) and percentage crystallisation (%X_c) are presented in Table 2 It can be inferred from Table 2 that the ΔH_{cc} and ΔH_m for PLA/MD-1 composite are significantly higher as compared to PLA. A slight increase of crystallinity is recorded for 1, 3 and 5 wt% loadings of MD in the PLA matrix showing %X_c = 15.50,

16.3, 11.8% respectively, as compared to neat PLA (10.9%). However, PLA/MD-10 film recorded only 5.66% crystallinity. Moreover, the incorporation of graphene oxide/carbon nanotube filler in PLA reported increased crystallisation and nucleation in the composites [34]. With further increment in the wt% loadings of MD, the %X_c shows decreasing trend, which is corroborated to the broadening and shifting of T_{cc} to higher temperature region. Therefore, the DSC results show slight enhancement in the crystallinity for PLA upon the addition of MD (1 wt%).

XRD Analysis

Figure 3 shows the X-ray diffractograms for MD, PLA and PLA/MD composites. It can be seen from Fig. 3a that the menadione exhibits an intense peak at $2\theta = 11.8°$ and several additional peaks in the 2θ regime of 15°–30°, which is in agreement with the XRD pattern obtained for menadione in earlier report [35]. It can be seen from Fig. 3b that the PLA represents the characteristic peak at $2\theta = 16.8°$ corresponding to the reflections obtained from (1 1 0)/(2 0 0) planes, which confirms the orthorhombic α-crystalline phase [36]. The less intense peaks noticed at $2\theta = 14.9°$, 19.2°, and 22.6° corresponds to the reflections obtained from (0 1 0), (2 0 3) and (2 1 0) planes, respectively. This in turn confirms the α-phase of PLA biopolymer. The XRD pattern obtained for PLA represents the α-crystalline structure [37]. After addition of MD in the PLA matrix, the characteristic peak for PLA at $2\theta = 16.8°$ remains to be unaltered which indicates that the lattice parameters and crystal structure are not affected.

Fourier Transform Infrared (FTIR) Spectroscopy

The FTIR spectrum obtained for food additive MD is represented in Fig. 4a. It can be seen from Fig. 4a that the appearance of peak positions at 1670 and 1584 cm^{-1} corresponds to the stretching of C=C groups in MD [35]. The bending vibration of C–H group is confirmed by the presence of peak at 1440 cm^{-1}. The visualization of band position at 1259 and 1153 cm^{-1} is ascribed to the stretching vibration of –C–O groups present in the MD [35]. The band positions that appear at 889, 773 and 668 cm^{-1} corresponds to bending vibration of –C=C functional groups

Table 2 DSC results of PLA and PLA-MD composites

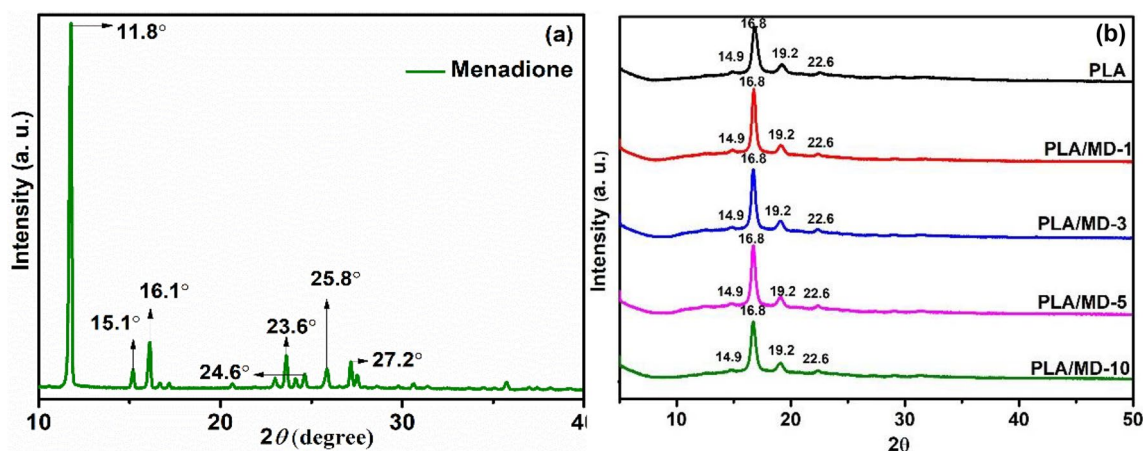| Samples	T_g (°C)	T_{cc} (°C)	T_m (°C)	ΔH_{cc}	ΔH_m	%X_c
PLA	62	97.5	173	5.26	15.40	10.9
PLA-MD-1	62	97.5	167.5	9.81	28.31	15.50
PLA-MD-3	61.8	97.5	167.5	16.87	32.01	16.30
PLA-MD-5	61.8	97.5	167.5	17.47	28.44	11.80
PLA-MD-10	57	126.6	167.5	14.18	19.45	5.66

Fig. 3 XRD pattern for **a** menadione and **b** PLA & PLA/MD composites
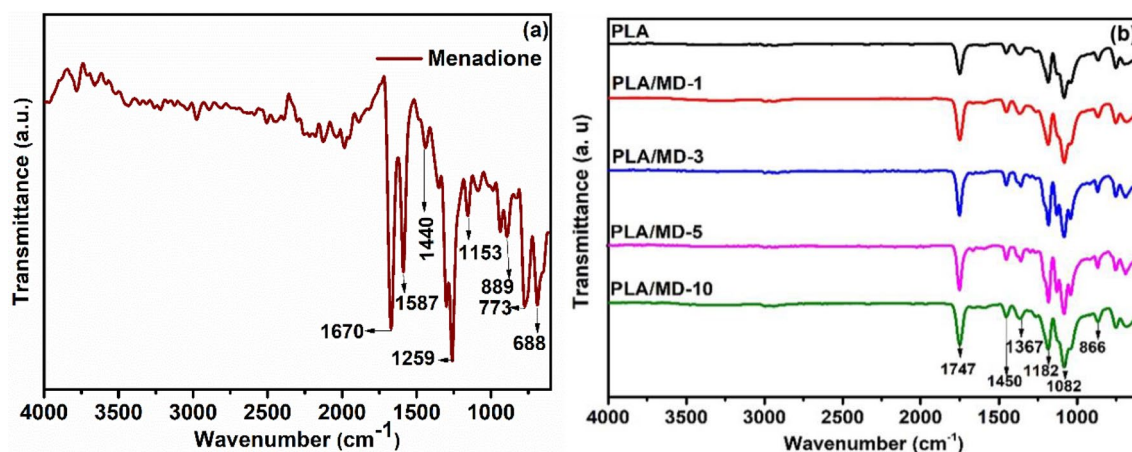

Fig. 4 FTIR spectra for **a** MD and **b** PLA & PLA/MD composites

in MD. The FTIR spectra obtained for PLA and PLA/MD composites are presented in Fig. 4b. It can be seen from Fig. 4b that the characteristic peak for PLA appears at 1754 cm^{-1} and this is attributed to the –C=O stretching of carbonyl backbone present in PLA [38]. The appearance of peak position at 1450 cm^{-1} represents the bending of methyl groups in PLA [39]. The presence of band position at 1367 cm^{-1} corresponds to the asymmetric bending of –CH– groups present in PLA [40]. The peak position identified at 1182 cm^{-1} is due to the asymmetric stretching of –C–O–C and rocking of –CH$_3$ groups present in PLA [38]. The band positions at 1082 cm^{-1} and 866 cm^{-1} are related to the stretching behaviour of –C–O and –C–C functional groups of PLA [38, 40]. Like PLA, the PLA/MD composites also share similar IR spectra since the characteristic peaks corresponding to the presence of MD are masked by PLA.

Morphology

The morphology obtained for MD, PLA and PLA/MD composites using FESEM analysis is depicted in Fig. 5. The FESEM image obtained for MD indicates rod-like morphology. The FE-SEM image obtained for PLA exhibits smooth and defect free surface. With respect to increase in wt% loadings of MD in the PLA matrix, agglomeration can be visualized from the FE-SEM images. Similar phenomenon is observed for PLA/curcumin composites, in which slight agglomeration is reported at higher loadings [26].

Transparency Analysis

In general, the UV–visible transparency measurements are deemed to be significant for any polymer composites films, since photo-chemical oxidation of food items occurs during storage upon exposure to UV–visible light. It is well known

**Fig. 5** FESEM micrographs of MD, PLA and PLA/MD composites
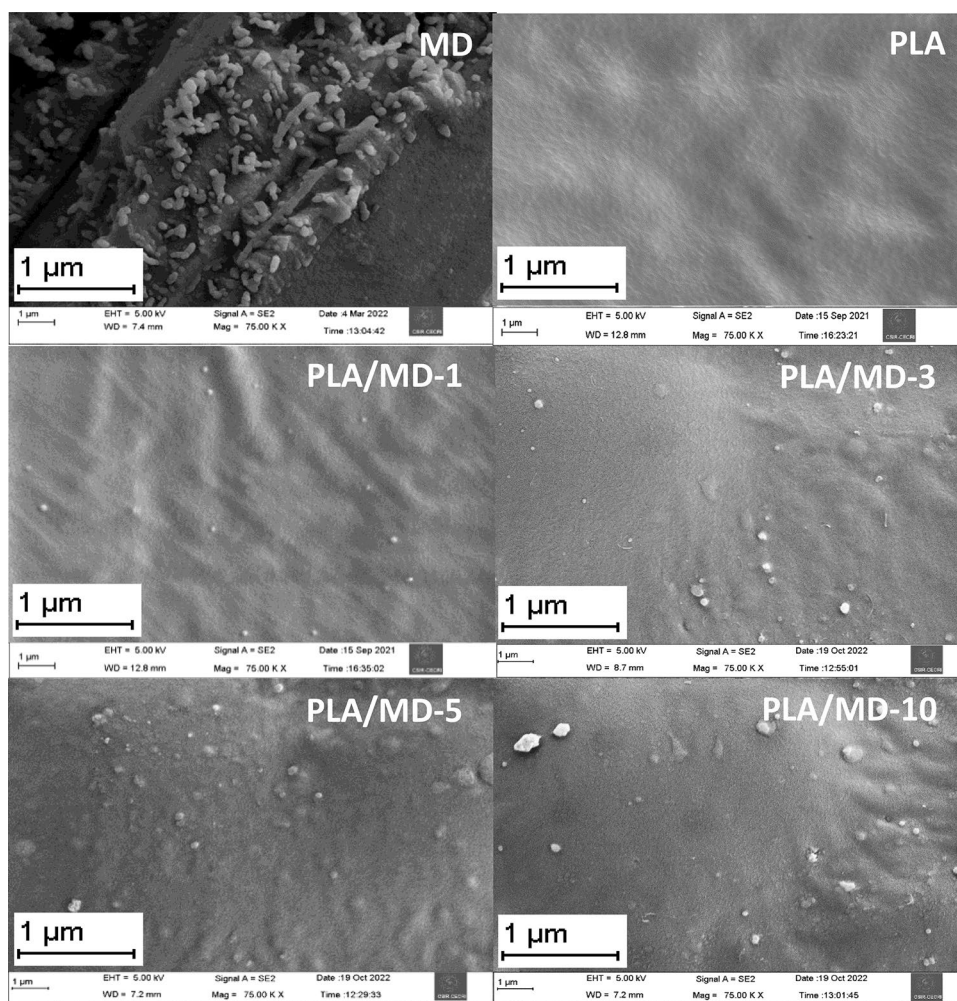
that UV regime is categorized into UV-A (400–315 nm), UV-B (280–315 nm) and UV-C (280–100 nm). Among them, UV-B is the most energetic and known to cause degradation of polymer and food spoilage [41]. In order to understand the UV blocking capability of biopolymer composites, transparency measurements are carried out for PLA and PLA/MD composites in the UV region [200–380 nm] and the spectra is portrayed in Fig. 6a. As can be deduced from the Fig. 6a, that PLA film exhibits higher rate of transmittance across the UV spectrum, which blocks only ~65% of UV-C, 47% of the high energy UV-B and 35% of UV-A light. This indicates that the PLA does not provide sufficient protection from UV light which could damage the food. However, in the case of PLA/MD composites, a general and incremental improvement in UV blockage is recorded in the important UV-B segment.

It can be seen from Fig. 6a that the PLA/MD-1 composite presents ~98% blockage in the UV-B regime. On the other hand, both the PLA/MD-5 and PLA/MD-10 composites exhibit ~100% hindrance in the UV-B regime. In order to better understand the efficiency of MD filler in terms of UV

blockage, UV protection factor (UPF) is calculated for PLA and PLA/MD composites following the procedure described in [42]. Accordingly, UPF rating is provided for samples based on UPF values as follows: In the case of PLA, the UPF value is obtained to be ~1.5. This indicates that PLA possesses poor UV protection property as the UPF value falls below 5. In the case of all the PLA/MD composites, the UPF value exceeds beyond 50 and hence can be rated as excellent UV absorbing biopolymer composite. The UPF values obtained for PLA and PLA/MD composites are in agreement with the earlier report documented for PLA/modified lignin composites for UV protection application [42]. Similar blockage of UV performance is shown by incorporation of coffee grounds in PLA matrix [43].

The PLA film shows high transparency in the visible region which is recorded to be ~75%. However, PLA/MD composites show decrement in transparency as compared to PLA with respect to wt% loadings of MD in the PLA matrix. The transparency for PLA/MD-1 composite in the visible regime is recorded to be ~52%. While, the PLA/MD-5 and PLA/MD-10 demonstrate ~32% and ~28% of

Fig. 6 a UV–Visible light transmission analysis and **b** contact transparency images for PLA as well as PLA/MD composites
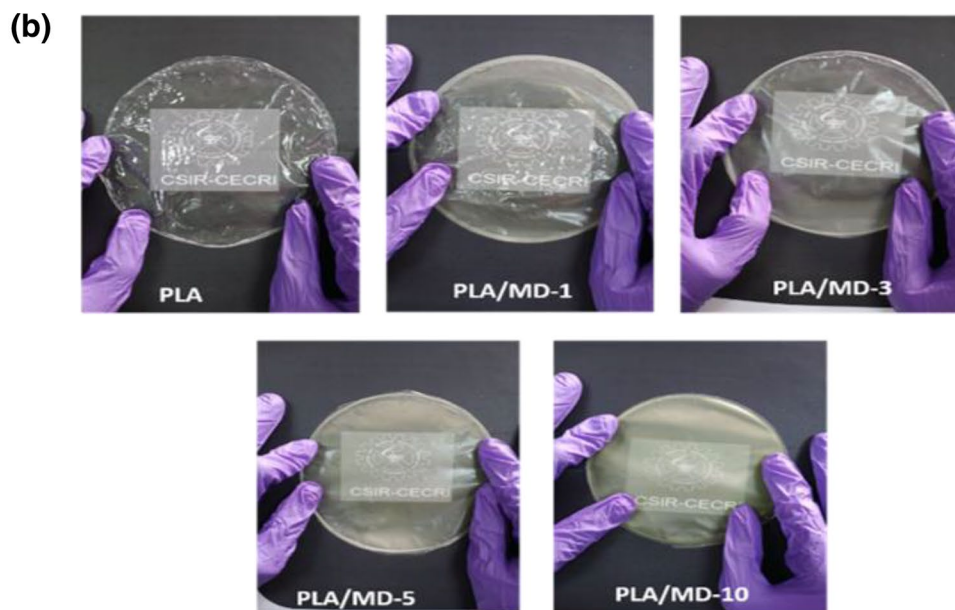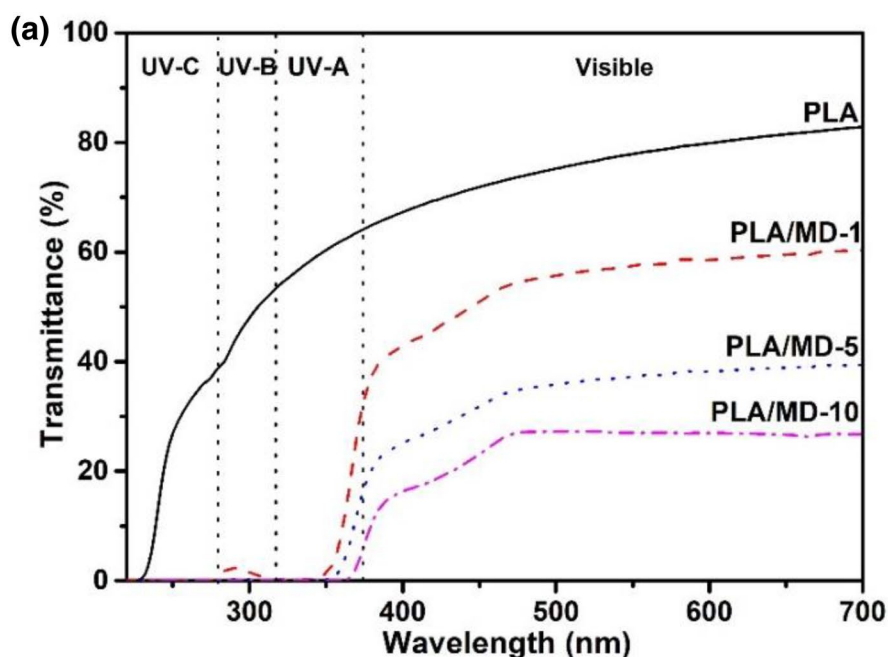
visible light transparency, respectively. The UV–Visible light transmission analysis result indicates that the PLA/MD composites can play vital role in the application of light sensitive food packaging material. Similar results have been reported for PLA/curcumin composite with similar UV blocking performance and visible light transmission property [26]. The contact transparency images obtained for PLA and PLA/MD composites is shown in Fig. 6b. The images illustrate high clarity for PLA as compared to PLA/MD composites, which show slightly diminishing characteristic as the wt% loading of MD is increased in the PLA matrix.

Mechanical Properties

The stress–strain curve obtained for PLA and PLA/MD composite films is depicted in Fig. 7a. From the stress–strain curve, important mechanical properties like tensile strength, elongation-at-break (%) and Young's modulus are obtained for PLA as well as PLA/MD composites and the details can be visualized from Fig. 7b. The tensile strength for PLA is recorded to be ~ 26 MPa while the composites demonstrate slightly better performance. The PLA/MD-3 composite exhibits the best performance in terms of tensile strength (~ 38 MPa) with a significance of ($p < 0.0001$),
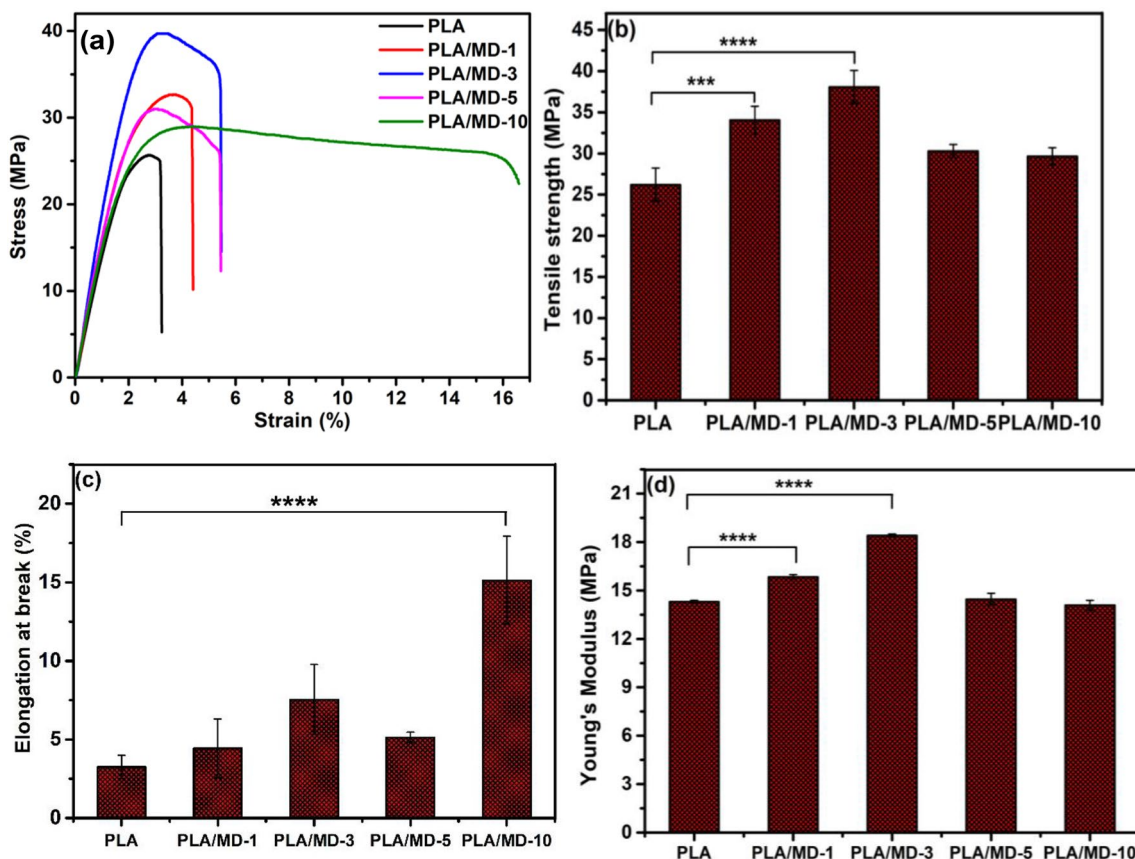
Fig. 7 **a** Stress–strain curve and **b** tensile strength, **c** elongation at break, **d** young's modulus for PLA as well as PLA/MD composites [$*p < 0.05$, $**p < 0.01$, $***p < 0.001$ and $****p < 0.0001$ (one-way ANOVA)]

which is closely followed by PLA/MD-1 composite. The least improvement in tensile strength (~ 29 MPa) is noticed for PLA-MD-10 composite as compared to neat PLA. This indicates good adhesion between MD and PLA matrix, at lower loadings of MD in the PLA matrix. The possible reason behind reduction in the tensile strength after 3 wt% loading of MD might be due to the agglomeration phenomenon. Similar results are reported for PLA/PVA blend mixtures by Restrepo et. al., [44].

Additionally, the elongation-at-break (%) for PLA and PLA/MD-10 composite is recorded to be ~ 3.2 and ~ 15%, respectively. The four-fold increment with significance of ($p < 0.0001$) in ductility exhibited by PLA/MD-10 composite is due to the plasticizing effect induced by MD. The increase in elongation-at-break (%) obtained for PLA/MD-10 composite is in accordance with the decrease in crystallinity recorded in DSC. This is in agreement with the DSC results, where shift in T_g to the lower side is noticed for PLA/MD-10 composite. The elongation-at-break (%) for PLA/polyphosphonate/graphene is reported by Jing *et. al.,* [45]. The Young's modulus is also found to be slightly have improved for PLA/MD-10 composites in comparison with PLA. The best performance in terms of Young's modulus is exhibited

by PLA/MD-3 composite with significance of ($p < 0.0001$), which is then followed by PLA/MD-1 and PLA/MD-5 composites. These results indicate that the composites at lower wt% loadings of MD can withstand more stretching pressure without deforming unlike PLA. Therefore, the improvement achieved in mechanical properties for PLA/MD composites is mainly due to the good interfacial adhesion among MD and the PLA matrix.

Oxygen Transmission Rate Analysis

The OTR results obtained for PLA and PLA/MD composites are presented in Fig. 8. The OTR value of the films is found out to be in correspondence with increase in wt% loadings of MD filler in the PLA matrix. The maximum reduction in the OTR (~ 30%) is exhibited by PLA/MD-5 composite in comparison with PLA. With further increment in loading, OTR is found to increase, which can be associated with agglomeration noticed for PLA/MD-10 composite in FE-SEM micrograph. The permeability of gases through PLA films is supported by tortuosity, which in turn is dependent on loading and orientation of the filler, adhesion between filler and the matrix [46]. The reduction in OTR recorded
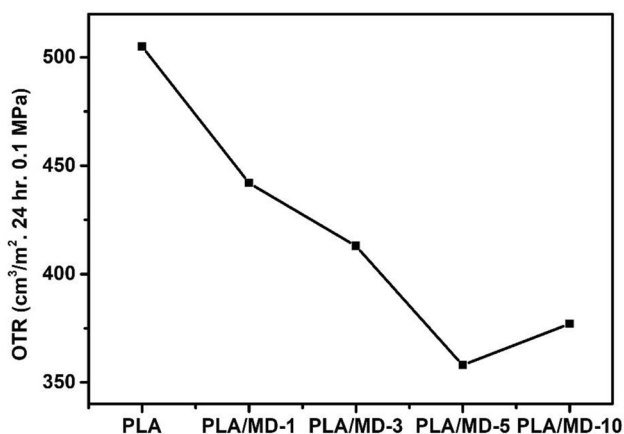
Fig. 8 Oxygen permeability measurements for PLA and PLA/MD composites
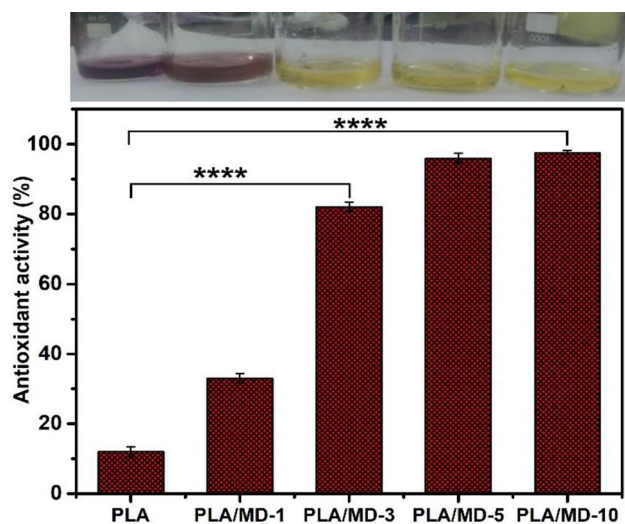
Fig. 9 Antioxidant activity of PLA and PLA/MD composite films [*$p < 0.05$, **$p < 0.01$, ***$p < 0.001$ and ****$p < 0.0001$ (one-way ANOVA)]

for PLA/MD composite film shows positive sign towards prevention of oxidative spoilage of food. The addition of reinforcements like silver nanoparticles has shown improvement in oxygen barrier property for PLA film [47].

Antioxidant Activity

In general, the antioxidants possess the capability to reduce DPPH by providing an electron or a hydrogen atom, resulting in 2,2-diphenyl-1-hydrazine (DPPH-H) or a substituted analogous hydrazine (DPPH-R) with a colourless or pale-yellow colour. The antioxidant activity of PLA and PLA/MD composite films is depicted in Fig. 9. It can be seen from Fig. 9 that the PLA film presents the least antioxidant

activity of ~ 10.7%. On the other hand, the PLA/MD composites shows robust performance with significance of ($p < 0.0001$) in terms of antioxidant activity with respect to increase in MD content. The maximum antioxidant activity of ~ 97% is exhibited by PLA/MD-10 composite film, which corresponds to ~ eightfold increment in radical scavenging activity in comparison with PLA biopolymer. The presence of methyl group in the MD helps in DPPH scavenging activity [21]. Thus, the PLA/MD composite films may find potential application in active food packaging for ensuring the extended shelf-life of stored food products.

Antibacterial Activity

The antibacterial activity of food packaging materials is crucial for preserving food quality while extending shelf life and preventing outbreaks of food-borne microorganisms. During the anti-bacterial studies, it is observed that PLA exhibits similar bacterial growth like control, which indicates the lack of anti-bacterial property for PLA [48]. Figure 10 depicts the antibacterial activity of PLA and PLA/MD composite films against *S. aureus* and *E. coli*. It can be seen from the Fig. 10 that all the PLA/MD composites showed antibacterial activity against *E. coli* and S. *aureus*. When 10 wt% of MD is incorporated in the PLA matrix, maximum inhibition (%) with significance of ($p < 0.0001$) is observed towards both *E. coli and S. aureus*. The antibacterial activity of MD is mainly due to its disruption of the bacterial membrane, causing damage to the essential elements required for membrane fluidity, such as loss of ions and reduced membrane potential, proteins, cytochrome C and radicals, which leads to the collapse of the proton pump. Further, MD can also exhibit anti-bacterial effect via depletion of adenosine triphosphate (ATP) as well as inhibition towards synthesis of cell wall and ribonucleic acid (RNA) [19]. The antibacterial activity exhibited by PLA/MD composite indicates that this formulation can be used as active food packaging material to hinder the development of microorganisms.

Migration Studies

The overall migration (OM) test is carried to evaluate the amount of non-volatile constituents which will migrate from PLA and PLA/MD composite films during dry food storage conditions and the results are displayed in Fig. 11. In this work, Tenax is used as dry food simulant in accordance to the (EU) No. 10/2011 regulations which set a maximum migration limit of ~ 10 mg/dm^2 of the proposed formulation for food packaging application. After incubation of the films for a period of 2 h at 70 °C, migration values of ~ 2 and ~ 2.6 mg/dm^2 are recorded for PLA and PLA/MD-1 composite, respectively. With respect to further increment
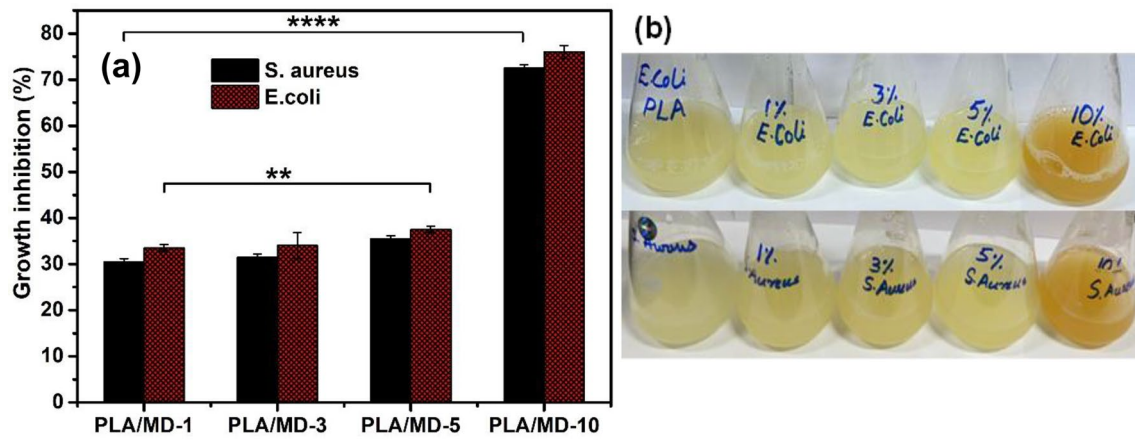
Fig. 10 a Antibacterial activity for PLA and PLA/MD composite films against *E. coli* and *S. aureus*. [*$p < 0.05$, **$p < 0.01$, ***$p < 0.001$ and ****$p < 0.0001$ (one-way ANOVA)]. **b** Pictorial antibacterial activity of PLA and PLA/MD composite films
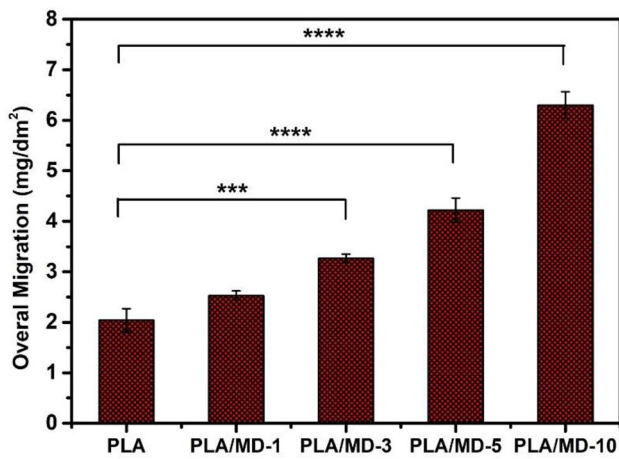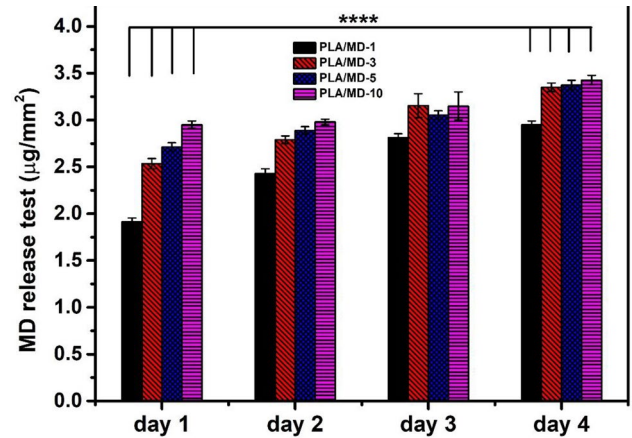

Fig. 11 Migration analysis for PLA and PLA/MD composite films using Tenax as dry food simulant [*$p < 0.05$, **$p < 0.01$, ***$p < 0.001$ and ****$p < 0.0001$ (one-way ANOVA)]

Fig. 12 Menadione release profile for PLA/MD composite films

in wt% loadings of MD in the PLA matrix, enhancement in the migration values can be noticed from Fig. 10. For PLA/MD-3, PLA/MD-5 and PLA/MD-10 composite films, the migration values are recorded to be ∼ 3.26, 4.22 and 6.40 mg/dm^2, respectively. The highest significance ($p < 0.0001$) is recorded for 5 and 10 wt% loadings of MD in the PLA matrix. The quantified OM values are found to be lower than the set limit of 10 mg/dm^2 by EU pointing to the suitability of PLA/MD composite films for dry food packaging application [46].

Menadione Release Test

The release of MD into distilled water from PLA/MD composite films is shown in Fig. 12. The release of MD is slower and unnoticeable during the initial phase and the release started only after few hours. The amount of release is found to be dependent on the concentration of MD filler in the PLA matrix. The PLA/MD-1 composite film shows the least release as envisaged, recording ∼ 1.22, 2.12, 2.19 and 2.32 µg/mm^2 from day 1-day 4, respectively. The highest release of MD is accordingly recorded for 10 wt% loading of MD in the PLA matrix with significance of ($p < 0.0001$) as can be seen from Fig. 12. The slower release of MD can be attributed to both the insolubility of PLA and MD in water. Further, the swelling phenomenon of PLA reduces the diffusion of MD into water medium. Generally, the release of reinforcing agents is governed by their diffusion and solubilisation in the polymer matrix [46]. Carbohydrate based polymers such as agar, chitosan carrageenan, and guar gum have been reported to have rapid release of reinforcing agents [49, 50].

Hydrolytic Degradation

Figure 13 depicts the hydrolytic degradation FE-SEM images of PLA and PLA/MD composite in acid and base environment. It can be seen from the Fig. 14 degradation is much faster in base environment than in acid environment at 35 and 55 ℃. In the case of base environment nearly 30% of weight loss occurred at the end of fifth day of degradation. The PLA/MD-10 composite demonstrates slightly higher weight loss compared to neat PLA in both 35 and 55 ℃ temperatures. In acidic solutions PLA and PLA/MD-10 exhibits nearly 11% of weight loss at the end of fifth day of analysis. The PLA/MD-10 in acidic solution also shows slightly faster degradation in comparison with neat PLA film. The FE-SEM images of PLA and PLA/MD-10 in acidic and basic solutions at 55 ℃ are shown in Fig. 14. It can be observed that the samples maintained in acidic condition shows the prevalence of holes on their surfaces which is contrast to the defect free surface seen in Fig. 5. This is associated with

erosion of the surface and leaching caused by the acidic medium. The samples in basic medium exhibits even more evident of hydrolytic degradation with the presence of cavity all over the surface of the films after 5 days. These cavities are more pronounced for PLA/MD-10 which suggest that the presence of MD support faster hydrolytic degradation. Further, neutral environment shows the least weight loss in comparison with the acid and base environment.

Conclusion

In the current work, menadione "MD" is envisaged as functional additive in the PLA matrix and its food packaging properties are investigated. The TGA analysis revealed that the incorporation of MD shows slight reduction in T_{max} for PLA. DSC analysis indicated the slower rate of crystallization process for PLA with respect to increase in MD loadings. This is because; the presence of MD in the PLA matrix
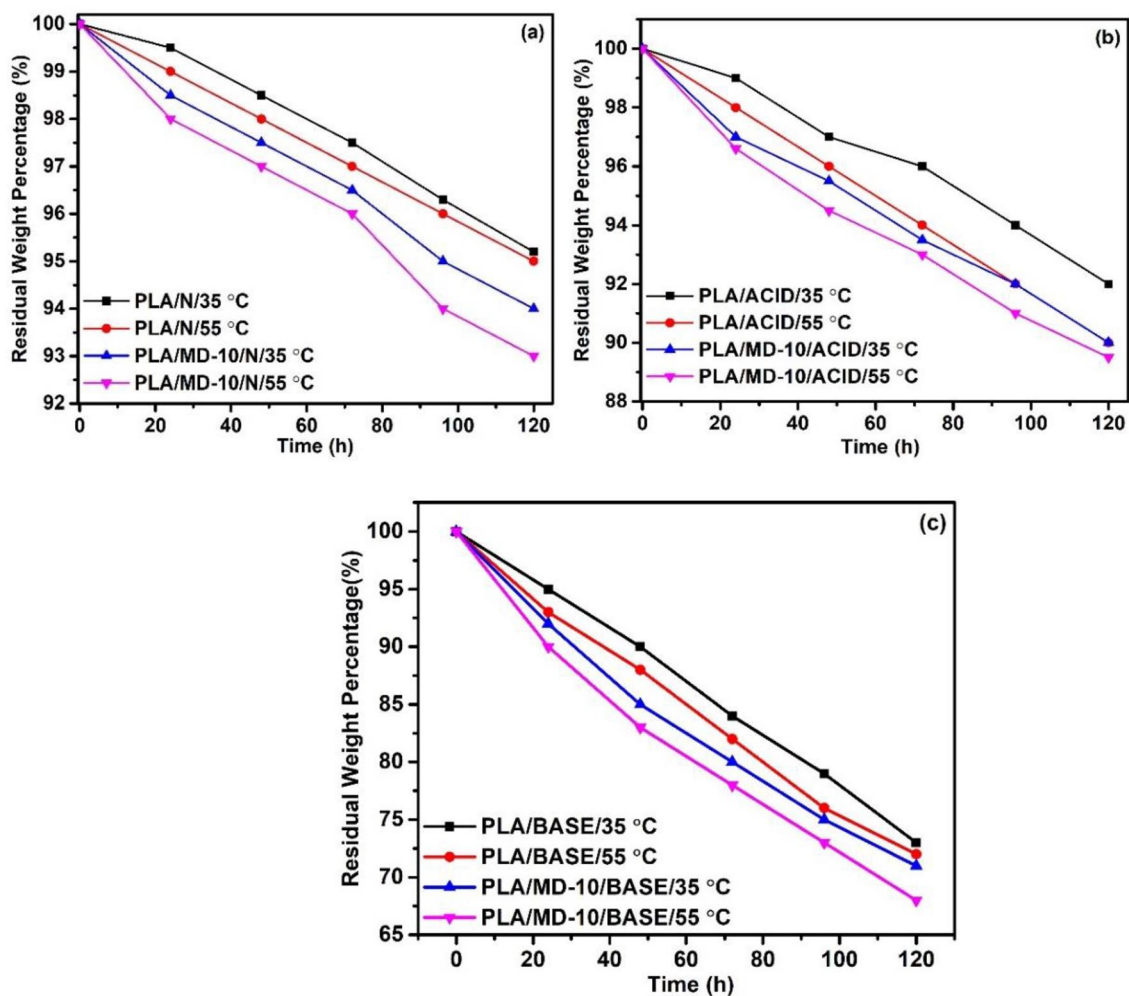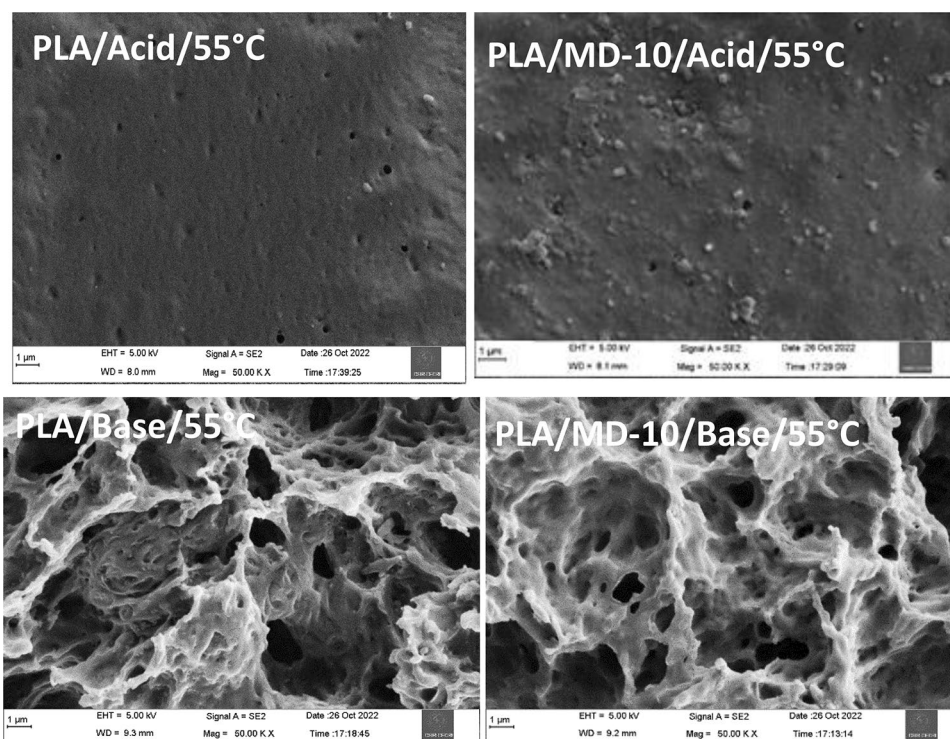

Fig. 13 Residual weight percentage of PLA and PLA/MD composite: **a** neutral, **b** acid and **c** base

Fig. 14 FE-SEM image of PLA and PLA/MD-10 composite film in acid and base environment

suppresses the diffusion rate of PLA chains to the surface of the nucleus and hence slows down the crystallization process. The XRD analysis confirmed the slight enhancement in the crystallinity (%) for PLA/MD composites. The PLA/MD-10 composite films showed complete blockage of UV light and presented the UPF value exceeding 50, which categorizes this formulation to be an excellent UV absorber suitable for packaging application. The addition of 10 wt% loading of MD in the PLA matrix resulted in considerable improvement of mechanical properties by enhancing the elongation-at-break (%) by four-fold with significance of ($p < 0.0001$) as compared to PLA. The PLA/MD-10 composite film is found to be effective in controlling the growth of food borne pathogenic bacteria (*E. coli* and S. *Aureus*). A noteworthy improvement in the DPPH scavenging activity is exhibited by PLA/MD-10 composite by recording ~ eightfold enhancement with significance of ($p < 0.0001$) in antioxidant property than PLA. The migration analysis carried out for PLA/MD composites revealed that the quantified OM values are found to be within the set limit of 10 mg/dm^2 by EU. The PLA/MD-10 composite film with excellent UV-blocking and antioxidant property along with enhanced ductility as well as antibacterial characteristics can find potential application as active food packaging material.

Author Contributions UL: experiments, characterization, data collection, formal analysis, validation and preparation of original draft. VR: characterization, analysis, writeup—review & editing. SL: resources and writeup—review and editing. RBV: conceptualization, supervision, resources, writeup—review and editing and funding acquisition.

Declarations

Competing interests The authors declare no competing financial interests.

References

1. Scalenghe R (2018) Resource or waste? A perspective of plastics degradation in soil with a focus on end-of-life options. Heliyon. https://doi.org/10.1016/j.heliyon.2018
2. Shamsuddin IM, Jafar JA, Shawai AS, Yusuf S, Lateefah M, Aminu I (2017) Bioplastics as better alternative to petroplastics and their role in national sustainability: a review. Adv Biosci Bioeng 5(4):63. https://doi.org/10.11648/j.abb.20170504.13

3. Groh KJ, Backhaus T, Carney-Almroth B, Geueke B, Inostroza PA, Lennquist A, Leslie HA, Maffini M, Slunge D, Trasande L, Warhurst AM, Muncke J (2019) Overview of known plastic packaging-associated chemicals and their hazards. Sci Total Environ 651:3253–3268

4. Tawakkal ISMA, Cran MJ, Miltz J, Bigger SW (2014) A review of poly(lactic acid)-based materials for antimicrobial packaging. J Food Sci. https://doi.org/10.1111/1750-3841.12534

5. Vatansever E, Arslan D, Nofar M (2019) Polylactide cellulose-based nanocomposites. Int J Biol Macromol 137:912–938

6. Getme AS, Patel B (2019) A review: Bio-fiber's as reinforcement in composites of polylactic acid (PLA). Mater Today. https://doi.org/10.1016/j.matpr.2020.02.457

7. Rasal RM, Janorkar AV, Hirt DE (2010) Poly(lactic acid) modifications. Prog Polym Sci (Oxford) 35:338–356

8. Zhou L, Ke K, Yang MB, Yang W (2021) Recent progress on chemical modification of cellulose for high mechanical-performance poly(lactic acid)/cellulose composite: a review. Compos Commun. https://doi.org/10.1016/j.coco.2020.100548

9. Jo MY, Ryu YJ, Ko JH, Yoon JS (2012) Effects of compatibilizers on the mechanical properties of ABS/PLA composites. J Appl Polym. https://doi.org/10.1002/app.36732

10. Byun Y, Rodriguez K, Han JH, Kim YT (2015) Improved thermal stability of polylactic acid (PLA) composite film via PLA-β-cyclodextrin-inclusion complex systems. Int J Biol Macromol 81:591–598

11. Pan F, Chen L, Jiang Y, Xiong L, Min L, Xie J, Qi J, Xiao H, Chen Y, de Hoop CF (2018) Bio-based UV protective films prepared with polylactic acid (PLA) and *Phoebe zhennan* extractives. Int J Biol Macromol 119:582–587

12. Shang H, Xu K, Li X, Lu S, Ke L, Yang H, Gao J, Tang D, Huang D, He X, Xu H, Shen B (2022) UV-protective and high-transparency poly(lactic acid) biocomposites for ecofriendly packaging of perishable fruits. Int J Biol Macromol 222:927–937

13. Ke L, Shang H, Tang M, Li X, Jiang L, Lu S, Tang D, Huang D, Zhu J, Liu C, Xu H, He X, Gao J (2022) High-heat and UV-barrier poly(lactic acid) by microwave-assisted functionalization of waste natural fibers. Int J Biol Macromol 220:827–836

14. Xu H, Shen M, Shang H, Xu W, Zhang S, Yang H, Zhou D, Hakkarainen M (2021) Osteoconductive and antibacterial poly(lactic acid) fibrous membranes impregnated with biobased nanocarbons for biodegradable bone regenerative scaffold. Ind Eng Chem Res 60:12021–12031

15. Shameli K, Ahmad MB, Yunus WM, Ibrahim NA, Rahman RA, Jokar M, Darroudi M (2010) Silver/poly (lactic acid) nanocomposites: preparation, characterization, and antibacterial activity. Int J Nanomed 5:573

16. Yang C, Zhu B, Wang J, Qin Y (2019) Structural changes and nano-TiO2 migration of poly(lactic acid)-based food packaging film contacting with ethanol as food simulant. Int J Biol Macromol 139:85–93

17. Shankar S, Rhim JW (2018) Preparation of antibacterial poly(lactide)/poly(butylene adipate-co-terephthalate) composite films incorporated with grapefruit seed extract. Int J Biol Macromol 120:846–852

18. Shankar S, Wang LF, Rhim JW (2018) Incorporation of zinc oxide nanoparticles improved the mechanical, water vapor barrier, UV-light barrier, and antibacterial properties of PLA-based nanocomposite films. Mater Sci Eng C 93:289–298

19. Andrade JC, Morais Braga MFB, Guedes GMM, Tintino SR, Freitas MA, Quintans LJ, Menezes IRA, Coutinho HDM (2017) Menadione (vitamin K) enhances the antibiotic activity of drugs by cell membrane permeabilization mechanism, Saudi. J Biol Sci 24:59–64

20. Chaitanya S, Singh I, Song JI (2019) Recyclability analysis of PLA/Sisal fiber biocomposites. Compos B Eng 173:106895

21. Xiangli L, Michael HA, William EA (2021) Descriptors for vitamin K3 (menadione); calculation of biological and physicochemical properties. J Mol Liq 330:115707

22. Sanjeev K, Satyendra G, Arun S (2013) Antimutagenic and antioxidant properties of plumbagin and other naphthoquinones. MRGTEM 755:30–41

23. Ewing DT, Vandenbelt JM, Oliver K (1939) The Ultraviolet absorption of vitamins K1, K2, and some related compounds. JBC 131:345–356

24. Song L, Meng Y, Wang X, Shi T, Wang Y, Shi Y, Liu LZ (2021) Crystallization, structure and significantly improved mechanical properties of PLA/PPC blends compatibilized with PLA-PPC copolymers produced by reactions initiated with TBT or TDI. Polymers. https://doi.org/10.3390/polym13193245

25. Arrua D, Strumia MC, Nazareno MA (2010) Immobilization of caffeic acid on a polypropylene film: synthesis and antioxidant properties. J Agric Food Chem 58:9228–9234

26. Roy S, Rhim JW (2020) Preparation of bioactive functional poly(lactic acid)/curcumin composite film for food packaging application. Int J Biol Macromol 162:1780–2178

27. Perotto G, Ceseracciu L, Simonutti R, Paul UC, Guzman-Puyol S, Tran TN, Bayer IS, Athanassiou A (2018) Bioplastics from vegetable waste: via an eco-friendly water-based process. Green Chem 20:894–902

28. Paul UC, Fragouli D, Bayer IS, Mele E, Conchione C, Cingolani R, Moret S, Athanassiou A (2017) Mineral oil barrier sequential polymer treatment for recycled paper products in food packaging. Mater Res Express. https://doi.org/10.1088/2053-1591/4/1/015501

29. Mcneill IC, Leiper HA (1985) Degradation studies of some polyesters and polycarbonates-2. Polylactide: degradation under isothermal conditions. Thermal Degrad Mech Photolysis Polym 11:309–326

30. Kopinke F, Remmler M, Mackenzie K, Milder M (1996) Thermal decomposition of biodegradable polyesters-11. Poly(lactic acid) 53:329–342

31. Khalili P, Liu X, Zhao Z, Blinzler B (2019) Fully biodegradable composites: thermal, flammability, moisture absorption and mechanical properties of natural fibre-reinforced composites with nano-hydroxyapatite. Materials. https://doi.org/10.3390/ma12071145

32. Xu H, Zhou J, Odelius K, Guo Z, Guan X, Hakkarainen M (2021) Nanostructured phase morphology of a biobased copolymer for tough and UV-resistant polylactide. ACS Appl Polym Mater 3:1973–1982

33. Valapa RB, Pugazhenthi G, Katiyar V (2015) Fabrication and characterization of sucrose palmitate reinforced poly(lactic acid) bionanocomposite films. J Appl Polym Sci. https://doi.org/10.1002/app.41320

34. Shang H, Ke L, Xu W, Shen M, Fan Z, Zhang S, Wang Y, Tang D, Huang D, Yang H, Zhou D, Xu H (2022) Microwave-assisted direct growth of carbon nanotubes at graphene oxide nanosheets to promote the stereocomplexation and performances of polylactides. Ind Eng Chem Res 61:1111–1121

35. Hassan GS (2013) Menadione. In Profiles of drug substances, excipients and related methodology. Academic Press Inc., Washington, DC. https://doi.org/10.1016/B978-0-12-407691-4.00006-X.

36. Dai X, Cao Y, Shi X, Wang X (2016) Non-isothermal crystallization kinetics, thermal degradation behavior and mechanical properties of poly(lactic acid)/MOF composites prepared by melt-blending methods. RSC Adv 6:71461–71471

37. Lv S, Gu J, Cao J, Tan H, Zhang Y (2015) Effect of annealing on the thermal properties of poly (lactic acid)/starch blends. Int J Biol Macromol 74:297–303

38. Papadopoulou EL, Paul UC, Tran TN, Suarato G, Ceseracciu L, Marras S, D'arcy R, Athanassiou A (2019) Sustainable active food packaging from poly(lactic acid) and cocoa bean shells. ACS Appl Mater Interfaces 11:31317–31327

39. Rocca-Smith JR, Lagorce-Tachon A, Iaconelli C, Bellat JP, Marcuzzo E, Sensidoni A, Piasente F, Debeaufort F, Karbowiak T (2017) How high pressure CO2 impacts PLA film properties. Express Polym Lett 11:320–333

40. Gupta A, Katiyar V (2017) Cellulose functionalized high molecular weight stereocomplex polylactic acid biocomposite films with improved gas barrier, thermomechanical properties. ACS Sustain Chem Eng 5:6835–6844

41. Sadeghifar H, Ragauskas A (2020) Lignin as a UV Light blocker-a review. Polymers (Basel). https://doi.org/10.3390/POLYM12051134

42. Kim Y, Suhr J, Seo HW, Sun H, Kim S, Park IK, Kim SH, Lee Y, Kim KJ, do Nam J (2017) All biomass and UV protective composite composed of compatibilized lignin and poly (lactic-acid). Sci Rep. https://doi.org/10.1038/srep43596

43. Xu H, Xie L, Li J, Hakkarainen M (2017) Coffee grounds to multifunctional quantum dots: extreme nanoenhancers of polymer biocomposites. ACS Appl Mater Interfaces 9:27972–27983

44. Restrepo I, Medina C, Meruane V, Akbari-Fakhrabadi A, Flores P, Rodríguez-Llamazares S (2018) The effect of molecular weight and hydrolysis degree of poly(vinyl alcohol)(PVA) on the thermal and mechanical properties of poly(lactic acid)/PVA blends. Polimeros 28:169–177

45. Jing J, Zhang Y, Tang X, Li X, Peng M, Fang Z (2018) Combination of a bio-based polyphosphonate and modified graphene oxide toward superior flame retardant polylactic acid. RSC Adv 8:4304–4313

46. Roy S, Rhim JW (2020) Curcumin incorporated poly(Butylene adipate-co-terephthalate) film with improved water vapor barrier and antioxidant properties. Materials 13:1–15

47. Fortunati E, Peltzer M, Armentano I, Jiménez A, Kenny JM (2013) Combined effects of cellulose nanocrystals and silver nanoparticles on the barrier and migration properties of PLA nano-biocomposites. J Food Eng 118:117–124

48. Taranamai P, Phinyocheep P, Panbangred W, Janhom M, Daniel P (2019) Antibacterial activity of sustainable composites derived from epoxidized natural rubber/silver-substituted zeolite/poly(lactic acid) blends. J Mater Sci 54:10389–10409

49. Roy S, Rhim JW (2020) Preparation of carbohydrate-based functional composite films incorporated with curcumin. Food Hydrocoll. https://doi.org/10.1016/j.foodhyd.2019.105302

50. Pramanik N, Mitra T, Khamrai M, Bhattacharyya A, Mukhopadhyay P, Gnanamani A, Basu RK, Kundu PP (2015) Characterization and evaluation of curcumin loaded guar gum/polyhydroxyalkanoates blend films for wound healing applications. RSC Adv 5:63489–63501